Accepted Manuscript

Removal of Cd2+, Ni2+ and PO43− from aqueous solution by hydroxyapatite-bentonite clay-nanocellulose composite

Sanna Hokkanen, Amit Bhatnagar, Varsha Srivastava, Valtteri Suorsa, Mika Sillanpää

PII: S0141-8130(17)34953-X
DOI: doi:10.1016/j.ijbiomac.2018.06.095
Reference: BIOMAC 9935

To appear in: *International Journal of Biological Macromolecules*

Received date: 12 December 2017
Revised date: 18 May 2018
Accepted date: 20 June 2018

Please cite this article as: Sanna Hokkanen, Amit Bhatnagar, Varsha Srivastava, Valtteri Suorsa, Mika Sillanpää , Removal of Cd2+, Ni2+ and PO43− from aqueous solution by hydroxyapatite-bentonite clay-nanocellulose composite. Biomac (2018), doi:10.1016/j.ijbiomac.2018.06.095

Removal of Cd^{2+}, Ni^{2+} and PO_4^{3-} from aqueous solution by hydroxyapatite-bentonite clay-nanocellulose composite

Sanna Hokkanen [1], Amit Bhatnagar [2], Varsha Srivastava [1], Valtteri Suorsa [3], Mika Sillanpää [1]

[1] Laboratory of Green Chemistry, School of Engineering Science, Lappeenranta University of Technology , Sammonkatu 12, FI-50130 Mikkeli, Finland, Phone: (+358) 40 747 7843, Fax (+358) 15-336-013 E-mail: Sanna.Hokkanen@lut.fi

[2] Department of Environmental and Biological Sciences, University of Eastern Finland, P.O. Box 1627, FI-70211, Kuopio, Finland

[3] Department of chemistry, Radiochemistry, University of Helsinki, A.I.Virtasen aukio 1, FI- 00014, Finland

Abstract

A novel hydroxyapatite-bentonite clay-nanocellulose (CHA-BENT-NCC) composite material was successfully prepared as adsorbent for the removal of Ni^{2+}, Cd^{2+} and PO_4^{3-} from aqueous solutions. Scanning electron microscopy (SEM), transmission electron microscopy (TEM), energy dispersive analysis of X-rays (EDAX), X-ray diffraction analysis (XRD) and Fourier-transform infrared spectroscopy (FTIR) were used for characterization of the adsorbent. The effect of pH, contact time, temperature, and initial adsorbate concentration were studied for optimization purpose. The adsorption behavior of the investigated ions were well described by the Freundlich adsorption model, and the maximum adsorption capacity for Ni^{2+}, Cd^{2+} and PO_4^{3-} was estimated to be 29.46 mmol/g, 10.34 mmol/g and 4.90 mmol/g, respectively. Desorption efficiency was achieved by treatment with 0.01 M HNO_3 for metals and 0.10 M NaOH for PO_4^{3-}. Five adsorption–desorption cycles were performed without significant decrease in adsorption capacities. The CHA-BENT-NCC material proved to be a very effective adsorption material for the treatment of mining water also from a copper mine in Finland.

Keywords

Composite material; hydroxyapatite-bentonite clay-nanocellulose (CHA-BENT-NCC); Adsorption isotherms; Metals and phosphate removal, Water treatment.

1. Introduction

There are currently 2.1 billion people around the world without safe drinking water at home and more than twice as many are without safe sanitation[1]. Anthropogenic activities, run off and unsafe disposal of toxic wastes are some of the main causes of water pollution. In addition to microbiological contaminants**,** nutrients (phosphorus and nitrogen) and heavy metals (cadmium, copper, chromium, nickel among others) are important water pollutants that cause problems to the environment and human beings [1-4]. Primarily, phosphorus can enter into freshwater ecosystems through agricultural runoff, domestic sewage and industrial effluents [5]. Nutrients cause the eutrophication in water bodies such as rivers and lakes [5]. Moreover, heavy metal contaminants in water environment have become a major problem due to their highly toxic nature and uncontrolled discharge to the environment [6-8]. It is acknowledged that the exposure to heavy metals may cause a wide range of health problems, including skin diseases, birth defects and cancer [9-11]. Because of this, the strict controls of various heavy metals in wastewaters are recommended by World Health Organization (WHO) [12].

Several technologies have been developed for removing harmful heavy metal contaminants and nutrients from water including physical, chemical, biological and a combination of different methods [11, 13, 14]. In recent years, adsorption as the alternative water treatment method has been study lively as it is recognized to be effective, efficient and inexpensive [5, 8, 11, 15]. Many different inorganic and organic adsorption materials such as minerals, zeolites, industrial by-products, agricultural wastes, biomass, polymeric materials and composite materials, have been investigated for metals and phosphate removal [5, 11, 16-18]. Inorganic−organic composite materials as adsorbents display more effective

properties than the inorganic and organic components individually due to their combined advantages[19, 20]. Our previous investigations indicate that calcium hydroxyapatite-microfibrillated cellulose (CHA/MFC) composites worked as effective adsorbents for metal, sulfates and nutrient removal from water [21-23]. Hydroxyapatite (CHA) is one of the most effective materials due to its capability for simultaneous removal of cationic and anionic contaminants from water [24-27]. Microfibrillated cellulose was used as the template to disperse CHA particles in the cellulose matrix for the preparation of composite materials.

In the present work, we synthesized CHA-BENT-NCC composite for the removal of anionic and cationic pollutants from water. The intrinsic properties of clays (specific surface area, excellent physical and chemical stability, high cation exchange capacity) enhance adsorption, structural and surface properties of the composites, synthesized in this study [28]. In addition to the well-known adsorption properties already known, the cost of clay is low, which makes it economically feasible[28]. The main aim of this work is therefore, to present a more effective, eco-friendly composite adsorbent material consisting of natural materials viz. calcium hydroxyapatite, bentonite clay and nanocellulose, for the removal of metals and phosphate from water.

2. Materials and methods

2.1. Raw material and chemicals

Nanocrystalline cellulose (AaltoCell^{TM}) was purchased from Aalto University. All used solutions were prepared in Millipore milliQ high-purity water. The chemicals used in this

study were supplied by Sigma–Aldrich (Germany). The metal stock solutions (1000 mg/L) were prepared by dissolving appropriate amounts of nickel nitrate salt ($Ni(NO_3)_2 \cdot 6H_2O$) and cadmium nitrate salts ($Cd(NO_3)_2 \cdot 4H_2O$) in deionized water. PO_4^{3-} stock solution (1000 mg/L) was prepared dissolving a dose of $NaHPO_4.7H_2O$ salt in deionized water. Adjustment of pH was accomplished using 0.1 M NaOH or 0.1 M HNO_3. Bentonite clay was supplied by Foodin Oy.

2.2. Synthesis of CHA-BENT-NCC

Nanocrystalline cellulose (3.2 g) and NaOH–thiourea solution containing NaOH (7.0 g), thiourea (12.0 g) and distilled water (100 mL) were mixed under magnetic stirring for 5 min at room temperature. The solution was then cooled to 5 ^{o}C for 12 h. For the synthesis of CHA-BENT-NCC composites, 0.110 g of $CaCl_2$ and 0.094 g of NaH_2PO_4 were added to the mixture of cellulose solution, distilled water (40 mL) and bentonite clay (3.0 g) under vigorous stirring. The mixture was then transferred into an oven at 90 ^{o}C for 6 h. The CHA-BENT-NCC material was washed four times in water and ethanol and was then centrifuged at 4000 rpm for 5 min. The synthesis route of CHA-BENT-NCC is illustrated in Figure 1.

2.3. Characterization of CHA-BENT-NCC

The surface functional groups of CHA-BENT-NCC composite material were identified by Fourier transform infrared spectroscopy (FTIR) (Vertex 70 by B Bruker Optics (Germany). An attenuated total reflection (ATR)-FTIR spectra was registered at 4 cm^{-1} resolution from 400 to 4000 cm^{-1} and 5 scans per sample. The morphology of the nanocellulose-bentonite particles was characterized with a Hitachi S-4800 field emission microscope (FESEM). XRD-measurements were carried out on a Philips PW1820 powder diffractometer equipped with Philips PW1710

diffractometer control unit and Siemens Kristalloflex X-ray generator. Copper Kα1 X-rays of wavelength 1.54 Å were used with a 2θ-angle step size of 0.04° and counting rate of 2.5 s per step over the total 2θ range of 7 to 70°. The particle diameter of hydroxyapatite-bentonite clay-nanocellulose composite was determined by transmission electron microscope (TEM) with the HITACHI 7700 operated at 100 kV.

2.4. Batch adsorption studies

Adsorption efficacy of CHA-BENT-NCC for Ni^{2+}, Cd^{2+} and PO_4^{3-} removal was studied by batch experiments. The adsorbent dose was 0.800 g/L and volume of Ni^{2+}, Cd^{2+} and PO_4^{3-} solutions was 0.005 L having concentrations ranging from 10 mg/L to 1000 mg/L. The effect of contact time was studied in reaction mixtures of 1.5 g/L of adsorbent and 50 mL of solution containing 500 mg/L of Ni^{2+}, Cd^{2+} and PO_4^{3-}. Agitation was performed under mechanical stirring and 2 mL samples were pipetted and styrene filtrated from the reaction mixtures at fixed intervals. The contact time was varied from 5 to 120 min. Batch experiments were performed at ambient temperature (i.e. 25^{o} C). The optimum conditions of all pertinent factors such as adsorbent dose, solution pH and contact time were used during the experiments. The metals and phosphate concentrations were analyzed by an inductively coupled plasma optical atomic emission spectrometry (ICP-OES) model iCAP 6300 (Thermo Electron Corporation, USA).

The adsorption capacity (q_e) was obtained by calculating the amount of ions adsorbed per mass unit of CHA-BENT-NCC (mmol/g) with the following formula:

$$q_e = \frac{C_i - C_e}{M} V. \quad (1)$$

where C_i is the initial metal/phosphate concentrations (mmol/L), and C_e is the equilibrium metal/phosphate concentrations (mmol/L), M is weight of the adsorbent (g) and V is the and the volume of the metal/phosphate solution (L).

2.6 Regeneration studies

To evaluate the reusability of CHA-BENT-NCC, regeneration of the spent adsorbents was also studied. At first, the adsorbent was loaded with studied ions by mixing 1.8 g/L of the adsorbent with 5 mL of 500 mg/L Ni^{2+}, Cd^{2+} and PO_4^{3-} solution. Metal ions were eluted using 0.10 M HNO_3 and PO_4^{3-} was eluted with 0.10 M NaOH. The regeneration efficiency (%RE) of the CHA-BENT-NCC adsorbent was calculated as follows:

$$(\%RE) = \frac{q_r}{q_0} \times 100 \quad (2)$$

where q_0 is the adsorption capacity (mmol/g) before regeneration and q_r is the adsorption capacity (mmol/g) after regeneration.

3. Results and discussions

3.1. Characterization studies

The FTIR spectrum (Figure 2) showed characteristic bands corresponding to the various functional groups in NCC and CHA-BENT-NCC. A strong peak in both spectrum bands at 3300

cm^{-1} is ascribed to O-H stretching. The peak at 2900 cm^{-1} is characteristic of C-H stretching in cellulose. The band at 1640 cm^{-1} could be ascribed to the H-OH bonding in water. The peak at 1063 cm^{-1} arises from the C-O-C pyranose ring skeletal vibration [22, 29, 30]. The peaks of CHA-BENT-NCC were observed at 1420 cm^{-1} and 880 cm^{-1} (the presence of CO_3^{2-}), 960-1025 cm^{-1} (the asymmetric and symmetric stretching vibrations of PO_4^{3-}) 795 cm^{-1} (Si-O Stretching), 695 cm^{-1} (Si-O deformation), 610 cm^{-1} (Al-O and Si-O out of plane vibration), 543 cm^{-1} (Al-O-Si deformation), 490 cm^{-1} (Si-O-Fe deformation), and 470 cm^{-1} (Mg-O deformation), respectively [31, 32]. It is noteworthy that the hydroxyl groups of the cellulose have an important role in interaction of CHA and bentonite on the surface of NCC.

For SEM analyses, the powdery samples were attached to a carbon tape and excess particles were removed with pressurized air. The samples were coated with 4 nm thick Au-Pd alloy by sputtering before the analysis. The SEM image illustrated, the nano size particles are stuck together to form aggregates of different sizes. The fibrous structure of cellulose does not appear in the images due to it can be assumed that the surface of the cellulose was completely covered by the bentonite clay and calcium hydroxyapatite layers. The contents of elements on the surface of the CHA-BENT-NCC in weight and atomic percentage values are supported by the EDX analysis (Figure 3). The relatively high concentrations of Ca, P, Si, Mg and Al are in line with the results of FTIR and conforms the adhesion of CHA and BENT in the hydroxyl groups of NCC.

For TEM analysis, the composite particles were first dispersed in ethanol and sonicated for 20 min to get suspensions of dispersed nanoparticles and then a drop of suspension was deposited on the carbon-coated copper grids (3 nm Carbon film, 400 Mesh). TEM images

were collected at different magnifications (from 25k to 50K). TEM images of synthesized composite are shown in Fig 4a and b. Particle diameter was found to be in the range of 15.4 nm to 26.5 nm having similar morphology.

The X-ray diffraction patterns were determined for identifying crystalline phases and chemical composition of the synthetized CHA-BENT-NCC composite material. Figure 5 shows clearly typical characteristic X-ray diffraction peaks for calcium hydroxyapatite, bentonite clay and nanocrystalline cellulose materials. The peaks at 2θ = 31, 32 and 33° on diffractogram are characteristic of the CHA and also some lower intensity secondary peaks located at 2θ = 26, 40, 47, and 49°, and other less intense located at 2θ = 29 and 54°, which confirm the presence of calcium hydroxyapatite [33]. The diffraction peaks at 2θ=20°, 35.0° and 62.0° indicate the existence montmorillonite in bentonite clay. The peaks at 2θ=26.3° and 2θ=28.1° are attributed to quartz compounds. The XRD pattern also indicated the presence of calcite 2θ=42.2° and feldspar 2θ=22.3° [34]. The peaks at 2ϑ = 14.6°, 16.8° and 22.7° are characteristic peaks of NCC [35].

3.2. Adsorption studies

3.2.1. Effect of pH and zeta-potential

The influence of pH on the adsorption of Cd^{2+}, Ni^{2+} and PO_4^{3-} was studied by conducting batch adsorption experiments at various pH values ranging from 2.0 to 10.0 with 300 mg/L solutions of adsorbates (Figure 6a). The adsorption efficiency was observed to increase from

62% to 93% for Cd^{2+}, from 65% to 91% for Ni^{2+} and from 45% to 82% for PO_4^{3-} with the increase of pH from 2.0 to 5.0. The wearable pH area for metal ion adsorption studies was found to be in the pH range 5-7. When pH was higher, the adsorption capacity increased due to the precipitation. Hydroxide precipitation for nickel occurs at pH ranging from 10 to 11 and cadmium precipitate as hydroxide at pH ranging from 8 to 11 [22]. In the case of PO_4^{3-}, the highest adsorption capacity was at pH-values ranging between 5.5-6.5. The adsorption capacity of PO_4^{3-} decreases in alkaline conditions. Zero point charge (pzc) of the adsorbent at pH 6.5 implies that, at pH < 6.5, the surface is positively charged and, at pH > 6.5, it is negatively charged (Figure 6b). At pH > 6.5, both the surface of CHA-BENT-NCC and PO_4^{3-} -ions are negatively charged and the net interaction is that of electrostatic repulsion. At pH < 6.5, the surface of the adsorbent is positive and the negative PO_4^{3-} ions are adsorbed through a favorable electrostatic attraction. In the case of metals, the effect of surface charge is the opposite: at alkaline conditions negatively charged surface can have electrostatic interactions with positive metal ions. In addition, the rise in metal ion sorption at the pH range 5-7 may causes ion exchange reaction: the positively charged metal ions in solution may exchange with H^+ from hydroxyl groups of the CHA-BENT-NCC surface. The functional groups that are involved in adsorption are: $\equiv CaOH^0$, $\equiv POH^0$ on surface of calcium hydroxyapatite; $\equiv SiOH^0$, $\equiv MeOH^0$ (Me: metal such as Fe, Al, Mg) on the surface of bentonite, $\equiv OH^0$, $\equiv COOH^0$ on the surface of cellulose. The pH conditions of the solution determines the charge of these groups [32].

3.2. Effect of contact time

The effect of contact time on the adsorption of Cd^{2+}, Ni^{2+} and PO_4^{3-} in aqueous solution is presented in Figure 5. The adsorption studies were conducted for 120 min. It was observed that the adsorption capacity of Cd^{2+}, Ni^{2+} and PO_4^{3-} increased rapidly with increasing the contact time and the adsorption equilibrium of $Cd^{2+}$and Ni^{2+} was achieved within the first 5 minutes. The adsorption equilibrium of PO_4^{3-} was reached within the first 12 minutes. Kinetic modelling of the adsorption was tested using the pseudo-first-order and pseudo-second-order models. The non-linear pseudo-first order model can be expressed as follows [36, 37]:

$$q_t = q_e(1 - e^{-k_1 t}) \quad (3)$$

The pseudo-second-order model, which assumes that the rate-determining step may be a chemical surface reaction, can be presented as follows [36, 37]:

$$q_{t=} \frac{k_2 q_e^2}{(1+k_2 q_e t)} t \quad (4)$$

where q_t (mmol g^{-1}) is the amount of adsorbed Ni^{2+}, Cd^{2+} and PO_4^{3-} at time t (min) and q_e (mmol g^{-1}) is the amount of adsorbates at equilibrium, k_1 (1/min) and k_2 (g/mmol min) are the rate constants of pseudo-first and pseudo-second order kinetic models, respectively.

The curves of the pseudo-first-order kinetic model and the pseudo-second-order kinetic models are shown in Figure 7 and the kinetic parameters are calculated and presented in

Table 1. The correlation coefficient (R^2) of the pseudo-first-order kinetic model for Cd^{2+}, Ni^2 was low and because of that the adsorption process cannot be explained by the pseudo-first-order kinetic model. Higher R^2 value of the pseudo-second-order kinetic model and the close correlation between the experimental (q_e) and calculated (q_t) values confirms the applicability of pseudo-second-order kinetic model in the adsorption of $Cd^{2+}$and Ni^{2+}using CHA-BENT-NCC. Thus, the adsorption process of Cd^2 and Ni^{2+} follows the pseudo-second-order kinetic model and the rate-limiting step of the adsorption mechanism is chemisorption. Moreover, the initial adsorption rate was 12.40 mmol/g min for Cd^{2+} and 4.20 mmol/ g min for Ni^{2+}.

In the case of PO_4^{3-}, there was no significant difference with the correlation coefficient (R^2) of the pseudo-first-order and pseudo-second-order kinetic models, but there is better correlation between the calculated q_t values from the pseudo-second-order model and the experimental q_e values (Table 1). In any case, the correlation is poor with both kinetic models and it is hard to say which one is better. The initial adsorption rate (0.27 mmol/g min), was much lower than adsorption rate of Cd^{2+}- and Ni^{2+} -ions.

3.3 Adsorption isotherms

Several adsorption isotherm models have been developed to represent liquid phase adsorption equilibrium data. Langmuir and Freundlich adsorption isotherms are the most commonly used models [38, 39]. The Langmuir adsorption isotherm is based on the assumption of monolayer and homogeneous surface consisting of a certain number of

active sites, each site can hold only one molecule while the Freundlich isotherm is an empirical model for heterogeneous systems[37, 38, 40]. Langmuir (Eq. 5.) model can be mathematically expressed as follows:

$$q_e = \frac{q_{max} K_L C_e}{1+K_L C_e} \quad (5)$$

where q_e (mmol/g) is the equilibrium adsorption capacity and q_m (mmol/g) is the maximum amount of the ions adsorbed per unit weight of the adsorbent. The Langmuir equilibrium constant, K_L (L/mmol), related to the affinity of the binding sites and describes the binding energy of the adsorption reaction between adsorbed molecules and adsorbent[22, 37].

The essential characteristic of the Langmuir isotherm on the nature can be assessed by a dimensionless equilibrium parameter:

$$R_L = \frac{1}{1+K_L C_i} \quad (6)$$

where R_L is a dimensionless equilibrium parameter or the separation factor and C_0 is the initial concentration of adsorbate solution (mmol/L). The value of R_L denotes the adsorption nature to be unfavorable ($R_L > 1$), favorable ($0 < R_L < 1$), irreversible ($R_L = 0$), or linear ($R_L = 1$).

The Freundlich model is given as:

$$q_e = K_f C_e^{1/n_F} \quad (7)$$

At equilibrium conditions, q_e is the amount of solute adsorbed and C_e is raised to the power of $1/n_F$. K_F is a relative indicator of adsorption capacity, while the dimensionless $1/n_F$ indicates the energy or intensity of the reaction and suggests the favorability and capacity of the adsorbent/adsorbate system[23, 37]. According to the theory, $n_F > 1$ represents favorable adsorption conditions.

The results in Table 2 show that the q_m value of Ni^{2+} (estimated by the Langmuir model) does not correspond to the experimentally obtained $q_{m,exp}$ value as well as the value of Cd^{2+} and PO_4^{3-}.

Figure 8 shows that the Freundlich isotherm fits better with the experimental data than Langmuir, and especially for Ni^{2+}, the adsorption was also supported by high R^2 value (Table 2). Relatively poor correlation coefficients of the Langmuir model (R^2 value < 0.99) indicates complex structure of the adsorbent surface and that the active sites are not similar, which is the assumption of Langmuir model. Hence, it can be assumed that adsorption process took place on a heterogeneous surface. These results are also in line with the results of characterization studies that demonstrated that there are different functional groups on the surface of CHA-BENT-NCC, which can work as adsorption sites for investigated ions.

The poor fitting results of PO_4^{3-}ions may also be explained by the attractive and repulsive electrostatic interaction between the surface and adsorbates during the adsorption process due to there are both positive and negative functional groups on the surface of CHA-BENT-NCC (see section 3.1). Noteworthy, the surface of CHA-BENT-NCC is negatively charged under the experimental conditions and a repulsive electrostatic interaction may experience between the anionic PO_4^{3-} ions and the surface before the adsorption.

According to the Eq. (5), the R_L values are < 0.14 for Cd^{2+}, < 0.71 for Ni^{2+} and < 0.81 for PO_4^{3-}, indicating that the adsorption process is favorable. Furthermore, the Freundlich constant n is greater than 1 which indicates a favorable condition for adsorption. The maximum adsorption capacity ($q_{m,exp}$) can reach upto 22.96 mmol/g for Ni^{2+}, 9.71 mmol/g for Cd^{2+} and 3.90 mmol/g for PO_4^{3-}. Comparison of the maximum metal and phosphate adsorption capacities for some cellulose based materials are presented in Table 3.

3.4 Effect of temperature

There are several thermodynamic parameters such as standard free energy (ΔG°), enthalpy (ΔH°) and entropy (ΔS°), which are associated with temperature dependence of the adsorption process. These parameters are used to define whether the process is endothermic or exothermic, spontaneous or nonspontaneous. The standard free energy change (ΔG°) can be calculated from the following equation [30]:

$$\Delta G^0 = -RTlnK_\alpha \qquad (8)$$

where R is the universal gas constant (8.314 J/mol K), T is the temperature (in Kelvin) and K° is the adsorption equilibrium constant. Values of lnK° are obtained by plotting lnK_d ($K_d = q_e/C_e$) versus C_e and extrapolating C_e to zero, the value of Y-axis was the value of ln K°. The standard enthalpy change (ΔH°) and the standard entropy (ΔS°) are calculated for Cd^{2+}, Ni^{2+} and PO_4^{3-} from the linear plot of ln K° versus 1/T in the following equation:

$$lnK_\alpha = \frac{\Delta H^0}{RT} + \frac{\Delta S^0}{R} \qquad (8)$$

The thermodynamic parameters of the Cd^{2+}, Ni^{2+} and PO_4^{3-} adsorption on CHA-BENT-NCC are presented in Table 4. The positive ΔH° value suggests that the adsorption on the CHA-BENT-NCC surface was an endothermic process [22, 41].

The negative values of ΔG^{o} implied the spontaneous adsorption process and the rise in temperature increases the degree of spontaneity of reaction. The positive values of ΔH^{o} indicated that the adsorption process was endothermic in nature, and as a result, adsorption capacity increased with an increase in temperature. Moreover, the positive value of ΔS^{o} showed the increased randomness for the overall adsorption process at the solid-solution interface. Accordingly, the van't Hoff plot gave a good linearity with the correlation coefficient (Table 3). Thus, adsorption was expected to occur spontaneously at cooler conditions than normal room temperature (290 K), relatively typical room temperature (296 K), and warm temperature (308 K) according to the thermodynamic parameters: $\Delta G^{o} < 0$, $\Delta H^{o} > 0$, and $\Delta S^{o} > 0$. At all temperatures, $|\Delta S^{o}|$ was found to be greater than $|\Delta H^{o}|$ indicating that the adsorption of Ni^{2+}, Cd^{2+} and PO_4^{3-} was dominated by the entropic rather than enthalpy changes. The removal efficiency of CHA-BENT-NCC for Cd^{2+} remained almost the same, despite the change in temperature; in case of Ni^{2+} , the adsorption efficiency increased 1.6% when the temperature increased by 18 K. The change in temperature clearly affected the adsorption of PO_4^{3-} and adsorption efficiency increased by 18% as temperature increased from 290 K to 308 K.

3.5 Removal mechanism

The adsorption of metal ions and PO_4^{3-} by CHA-BENT-NCC occur via various possible mechanisms. The factors that influencing the absorption process may be related to the

characteristics of the binding sites (e.g. functional groups, structure, surface properties, etc.), the properties of the adsorbent (e.g. concentration, ionic size, ionic charge, molecular structure etc.) and the solution chemistry (e.g. pH, ionic strength, etc.). As mentioned previously, there are a large amount of potential adsorption sites for both cationic and anionic adsorbates on the surface of CHA-BENT-NCC.

In the case of $Cd^{2+}$and Ni^{2+}, ion-exchange between the calcium of and the bivalent ion is one potential removal mechanism. The metal ions replaces the calcium in the CHA lattice, according to the reaction [21]:

$$Ca_{10}(PO_4)_6(OH)_2 + xMe^{2+} \leftrightarrow (Ca_{10-x})Me_x(PO_4)_6\,(OH)_2 + xCa^{2+} \quad (9)$$

Another suggested mechanism with CHA is dissolution – precipitation. This reaction takes place in two steps: at first CHA is dissolved in solution followed by the reaction of the phosphate ion with the metal to form a new insoluble phase:

$$Ca_{10}(PO_4)_6(OH)_2 + 14H^+ \leftrightarrow 10Ca^{2+} + 6H_2PO_4^- + 2H_2O \quad (10)$$

$$10Me^{2+} + 6H_2PO_4^- + 2H_2O \leftrightarrow Me_{10}(PO_4)_6(OH)_2 + 14H^+ \quad (11)$$

Bentonite clay is consisting mostly of montmorillonite witch is hydrated sodium calcium aluminium magnesium silicate hydroxide ($(Na,Ca)_{0.33}(Al,Mg)_2(Si_4O_{10})(OH)_2{\cdot}nH_2O$)[42]. Ion exchange of $Cd^{2+}$and Ni^{2+}, for Ca^{2+} and Mg^{2+} ions of bentonite clay is also possible mechanism for metal ions removal. This process can be represented by following equations:

$$Ca_2Al_2SiO_7 + H_2O \rightarrow SiO_2 + Al(OH)_3 + 2Ca^{2+} + 4OH \quad (12)$$

$$2CaO \cdot SiO_2 + 2H_2O \rightarrow 2Ca^{2+} + H_4SiO_4 + 4OH^- \quad (13)$$

$$Me^{2+} + 2OH^- \rightarrow MeOH_2 \quad (14)$$

$$2Me^{2+} + SiO_4^{4-} \rightarrow Me_2SiO_4 \quad (15)$$

The adsorption of ions on bentonite in acidic conditions can be described by following equation:

$$Si - OH \cdots H - O - H[Me(OH_2)_3]^{2+} \rightarrow Si - O - Me + H_3O^+ \quad (16)$$

This process is possible due to the ionization and hydrolysis of surfaces silanol sites (≡Si–OH) and aluminols (≡Al–OH) [43].

The adsorption of PO_4^{3-}-ions on CHA can be explained as exchange of ions reaction between OH^--ions and $H_2PO_4^-$-ions. The adsorption by CHA may also involve electrostatic attraction between positive charged Ca^+ and hydroxyl bonding formation. Al-OH and Si-OH may be the most dominated group that caused the phosphate adsorption on bentonite. The assumed adsorption process of phosphate can be represented as:

$$\equiv Si - OH + H_2PO_4^- \rightarrow (\equiv Si)_2HPO_4 + H_2O + OH^- \quad (17)$$

$$\equiv Al - OH + H_2PO_4^- \rightarrow (\equiv Al)_2HPO_4 + H_2O + OH^- \quad (18)$$

In alkaline conditions chemical precipitation between phosphate and these cations, forming $Ca_3(PO_4)_2$ and $Mg_3(PO_4)_2$ may also attend to removal process [44].

3.6 Regeneration studies

Regenerability of adsorbent is very important property from economy and environmental point of view [45]. Furthermore, it is important to find effective and nontoxic eluents for the quantitative recovery of metal ions. In this study, 0.1 M HNO_3 proved to be effective eluent for metals desorption and 0.1 M. NaOH for phosphate desorption. Figure 9 shows that after five cycles, the adsorption capacity of CHA-BENT-NCC was decreased from 97% to 74% for Cd^{2+} and from 98% to 80% for Ni^{2+}, and form 75% to 68% for PO_4^{3-}.

3.7 Testing of CHA-BENT-NCC with mining water from copper mine

To see the practical applicability, the efficiency of CHA-BENT-NCC was tested for the removal of metals from mining water from the copper mine in Finland. The composition of the mining wastewater before and after adsorption studies is depicted in Table 4. Mine water treatment is a very complex process and it is affected by many factors, such as waters matrices, composition and pH [46]. The experiments were implemented using the same batch studies conditions described above, at ambient temperature and pH 3.2. The results of the adsorption study showed that CHA-BEN-NCC effectively removed other metal ions also (present in mining water), in addition to Ni^{2+} (Table 5.)

4. Conclusions

The present study focused on the adsorption of Ni^{2+}, Cd^{2+} and PO_4^{3-} from aqueous solution using the CHA-BENT-NCC as adsorbent. The synthesized adsorbent was found very effective and maximum adsorption capacities were recorded as 22.96 mmol/g for Ni^{2+}, 9.71 mmol/g for Cd^{2+} and 3.96 mmol/g for PO_4^{3-}. The adsorption was shown to be dependent on the solution pH, and the optimum pH value for the adsorption was around 5 for metals and PO_4^{3-}. The kinetic study demonstrated poor correlation (R^2) with both the pseudo-first-order kinetic model and the pseudo-second-order kinetic model for all investigated ions. The kinetics of metals followed pseudo-second-order model better. In case of PO_4^{3-}, the result was tolerably the same for both models. Calculated thermodynamic parameters showed that the adsorption process was endothermic for all investigated ions. In the isotherm studies, the Freundlich isotherm model provided the best fit to the experimental adsorption isotherm data for investigated ions. The adsorption/desorption cycle results demonstrated the regenerability of adsorbent up to 5 cycles. The CHA-BENT-NCC material proved to be very effective adsorption material for metals and phosphorus contaminated water, as well as mining water from the copper mine of Finland.

Acknowledgment

This research was funded by Maa- ja vesitekniikan tuki ry.

References:

[1] G. Cui, M. Liu, Y. Chen, W. Zhang, J. Zhao, Synthesis of a ferric hydroxide-coated cellulose nanofiber hybrid for effective removal of phosphate from wastewater, Carbohydrate Polymers, 154 (2016) 40-47.

[2] A.S. Ayangbenro, O.O. Babalola, A New Strategy for Heavy Metal Polluted Environments: A Review of Microbial Biosorbents, International Journal of Environmental Research and Public Health, 14 (2017) 94.

[3] W.H.O.s.W.G.f.d.-w.q. (GDWQ), (2017).

[4] H. Sehaqui, A. Mautner, U. Perez de Larraya, N. Pfenninger, P. Tingaut, T. Zimmermann, Cationic cellulose nanofibers from waste pulp residues and their nitrate, fluoride, sulphate and phosphate adsorption properties, Carbohydrate Polymers, 135 (2016) 334-340.

[5] M.S. Sivakami, T. Gomathi, J. Venkatesan, H.-S. Jeong, S.-K. Kim, P.N. Sudha, Preparation and characterization of nano chitosan for treatment wastewaters, Int. J. Biol. Macromol., 57 (2013) 204-212.

[6] S. Hokkanen, E. Repo, T. Suopajärvi, H. Liimatainen, J. Niinimaa, M. Sillanpää, Adsorption of Ni(II), Cu(II) and Cd(II) from aqueous solutions by amino modified nanostructured microfibrillated cellulose, Cellulose, 21 (2014) 1471-1487.

[7] N.A. Fakhre, B.M. Ibrahim, The use of new chemically modified cellulose for heavy metal ion adsorption, Journal of Hazardous Materials, 343 (2018) 324-331.

[8] C. Li, M. Zhang, H. Zhong, H. He, Y. Feng, X. Yin, Synthesis of a bioadsorbent from jute cellulose, and application for aqueous Cd (II) removal, Carbohydrate Polymers, 189 (2018) 152-161.

[9] B. Zambelli, V.N. Uversky, S. Ciurli, Nickel impact on human health: An intrinsic disorder perspective, Biochimica et Biophysica Acta (BBA) - Proteins and Proteomics, 1864 (2016) 1714-1731.

[10] J. Godt, F. Scheidig, C. Grosse-Siestrup, V. Esche, P. Brandenburg, A. Reich, D.A. Groneberg, The toxicity of cadmium and resulting hazards for human health, Journal of Occupational Medicine and Toxicology, 1 (2006) 22.

[11] T.A. Kurniawan, G.Y.S. Chan, W.-h. Lo, S. Babel, Comparisons of low-cost adsorbents for treating wastewaters laden with heavy metals, Sci. Total Environ., 366 (2006) 409-426.

[12] D.D. Mara, Water, sanitation and hygiene for the health of developing nations, Public Health, 117 (2003) 452-456.

[13] X. Lei, X. Dai, S. Long, N. Cai, Z. Ma, X. Luo, Facile Design of Green Engineered Cellulose/Metal Hybrid Macrogels for Efficient Trace Phosphate Removal, Industrial & Engineering Chemistry Research, 56 (2017) 7525-7533.

[14] D. Zhou, L. Zhang, J. Zhou, S. Guo, Cellulose/chitin beads for adsorption of heavy metals in aqueous solution, Water Research, 38 (2004) 2643-2650.

[15] M. Stephen, N. Catherine, M. Brenda, K. Andrew, P. Leslie, G. Corrine, Oxolane-2,5-dione modified electrospun cellulose nanofibers for heavy metals adsorption, Journal of Hazardous Materials, 192 (2011) 922-927.

[16] S. Srivastava, A. Kardam, K.R. Raj, Nanotech Reinforcement onto Cellulosic Fibers: Green Remediation of Toxic Metals, International Journal of Green Nanotechnology, 4 (2012) 46-53.

[17] Y. Shaoping, F. Shiyu, L. Hao, Z. Yiming, L. Xueyun, Hydrogel beads based on carboxymethyl cellulose for removal heavy metal ions, Journal of Applied Polymer Science, 119 (2011) 1204-1210.

[18] T. Xiong, X. Yuan, X. Chen, Z. Wu, H. Wang, L. Leng, H. Wang, L. Jiang, G. Zeng, Insight into highly efficient removal of cadmium and methylene blue by eco-friendly magnesium silicate-hydrothermal carbon composite, Applied Surface Science, 427 (2018) 1107-1117.

[19] B. Samiey, C.-H. Cheng, J. Wu, Organic-Inorganic Hybrid Polymers as Adsorbents for Removal of Heavy Metal Ions from Solutions: A Review, Materials, 7 (2014) 673.

[20] S.B. Khan, K.A. Alamry, H.M. Marwani, A.M. Asiri, M.M. Rahman, Synthesis and environmental applications of cellulose/ZrO2 nanohybrid as a selective adsorbent for nickel ion, Composites Part B: Engineering, 50 (2013) 253-258.

[21] S. Hokkanen, E. Repo, L.J. Westholm, S. Lou, T. Sainio, M. Sillanpää, Adsorption of Ni2+, Cd2+, PO43− and NO3− from aqueous solutions by nanostructured microfibrillated cellulose modified with carbonated hydroxyapatite, Chemical Engineering Journal, 252 (2014) 64-74.

[22] S. Hokkanen, A. Bhatnagar, E. Repo, S. Lou, M. Sillanpaa, Calcium hydroxyapatite microfibrillated cellulose composite as a potential adsorbent for the removal of Cr(VI) from aqueous solution, Chemical Engineering Journal, 283 (2016) 445-452.

[23] S. Hokkanen, A. Bhatnagar, A. Koistinen, T. Kangas, U. Lassi, M. Sillanpaa, Comparison of adsorption equilibrium models and error functions for the study of sulfate removal by calcium hydroxyapatite microfibrillated cellulose composite, Environ. Technol., (2017) Ahead of Print.

[24] J.F. Cawthray, A.L. Creagh, C.A. Haynes, C. Orvig, Ion Exchange in Hydroxyapatite with Lanthanides, Inorganic Chemistry, 54 (2015) 1440-1445.

[25] D.C. Manatunga, R. de Silva, K.M.N. de Silva, R. Ratnaweera, Natural polysaccharides leading to super adsorbent hydroxyapatite nanoparticles for the removal of heavy metals and dyes from aqueous solutions, RSC Advances, 6 (2016) 105618-105630.

[26] D.C. Manatunga, R.M. de Silva, K.M. Nalin de Silva, N. de Silva, E.V.A. Premalal, Metal and polymer-mediated synthesis of porous crystalline hydroxyapatite nanocomposites for environmental remediation, Royal Society open science, 5 (2018) 171557.

[27] M.S. Fernando, R.M. de Silva, K.M.N. de Silva, Synthesis, characterization, and application of nano hydroxyapatite and nanocomposite of hydroxyapatite with granular activated carbon for the removal of Pb2+ from aqueous solutions, Applied Surface Science, 351 (2015) 95-103.

[28] M.K. Uddin, A review on the adsorption of heavy metals by clay minerals, with special focus on the past decade, Chem. Eng. J. (Amsterdam, Neth.), 308 (2017) 438-462.

[29] N. Akartasse, E. Mejdoubi, B. Razzouki, K. Azzaoui, S. Jodeh, O. Hamed, M. Ramdani, A. Lamhamdi, M. Berrabah, I. Lahmass, W. Jodeh, S. El Hajjaji, Natural product based composite for extraction of arsenic (III) from waste water, Chemistry Central Journal, 11 (2017) 33.

[30] X. Yu, S. Tong, M. Ge, J. Zuo, Removal of fluoride from drinking water by cellulose@hydroxyapatite nanocomposites, Carbohydrate Polymers, 92 (2013) 269-275.

[31] K.S. Katti, D. Sikdar, D.R. Katti, P. Ghosh, D. Verma, Molecular interactions in intercalated organically modified clay and clay–polycaprolactam nanocomposites: Experiments and modeling, Polymer, 47 (2006) 403-414.

[32] A.S.K. Kumar, S. Kalidhasan, V. Rajesh, N. Rajesh, Application of Cellulose-Clay Composite Biosorbent toward the Effective Adsorption and Removal of Chromium from Industrial Wastewater, Ind. Eng. Chem. Res., 51 (2012) 58-69.

[33] S.-C. Liou, S.-Y. Chen, H.-Y. Lee, J.-S. Bow, Structural characterization of nano-sized calcium deficient apatite powders, Biomaterials, 25 (2004) 189-196.

[34] G.A. Ikhtiyarova, A.S. Özcan, Ö. Gök, A. Özcan, Characterization of natural- and organo-bentonite by XRD, SEM, FT-IR and thermal analysis techniques and its adsorption behaviour in aqueous solutions, in: Clay Minerals, 2012, pp. 31.

[35] A. Kljun, T.A.S. Benians, F. Goubet, F. Meulewaeter, J.P. Knox, R.S. Blackburn, Comparative Analysis of Crystallinity Changes in Cellulose I Polymers Using ATR-FTIR, X-ray Diffraction, and Carbohydrate-Binding Module Probes, Biomacromolecules, 12 (2011) 4121-4126.

[36] Y.S. Ho, G. McKay, Kinetic Models for the Sorption of Dye from Aqueous Solution by Wood, Process Safety and Environmental Protection, 76 (1998) 183-191.

[37] E. Repo, J.K. Warchol, T.A. Kurniawan, M.E.T. Sillanpää, Adsorption of Co(II) and Ni(II) by EDTA- and/or DTPA-modified chitosan: Kinetic and equilibrium modeling, Chemical Engineering Journal, 161 (2010) 73-82.

[38] I. Langmuir, The adsorption of gases on plane surfaces of glass, mica and platinum, J. Am. Chem. Soc., 40 (1918) 1361-1402.

[39] H. Freundlich, Colloid and Capillary Chemistry, E. P. Dutton & Co.

[40] H. Freundlich, Over the adsorption in solution, J. Phys. Chem, 57 (1906) 1100-1107.

[41] A. Halajnia, S. Oustan, N. Najafi, A.R. Khataee, A. Lakzian, Adsorption–desorption characteristics of nitrate, phosphate and sulfate on Mg–Al layered double hydroxide, Applied Clay Science, 80–81 (2013) 305-312.

[42] J. Alexander, Bentonite, Industrial & Engineering Chemistry, 16 (1924) 1140-1142.

[43] G. Chen, L. Shi, Removal of Cd(ii) and Pb(ii) ions from natural water using a low-cost synthetic mineral: behavior and mechanisms, RSC Advances, 7 (2017) 43445-43454.

[44] Y. Xue, H. Hou, S. Zhu, Characteristics and mechanisms of phosphate adsorption onto basic oxygen furnace slag, Journal of Hazardous Materials, 162 (2009) 973-980.

[45] R.K. Gautam, A. Mudhoo, G. Lofrano, M.C. Chattopadhyaya, Biomass-derived biosorbents for metal ions sequestration: Adsorbent modification and activation methods and adsorbent regeneration, Journal of Environmental Chemical Engineering, 2 (2014) 239-259.

[46] E. Iakovleva, E. Mäkilä, J. Salonen, M. Sitarz, S. Wang, M. Sillanpää, Acid mine drainage (AMD) treatment: Neutralization and toxic elements removal with unmodified and modified limestone, Ecological Engineering, 81 (2015) 30-40.

Figure 1. Synthesis route of CHA-BENT-NCC.

Figure 2. FTIR spectra of a) NCC and b) CHA-BENT-NCC.

Figure 3. SEM (a) and EDAX (b) analysis images of CHA-BENT-NCC.

Figure 4. TEM image of hydroxyapatite-bentonite clay-nanocellulose composite at different magnifications (a) 25k (b)50k

Figure 5. XRD analysis of CHA-BENT-NCC composite material.

Figure 6. The effect of pH (a) for adsorption and surface charge (b) of CHA-BENT-NCC (Adsorbent dose 0.800 g/L; time 12 h).

Figure 7a-c. The effect of contact time on the adsorption of a) Cd^{2+}, b) Ni^{2+} and c) PO_4^{3-} onto CHA-BENT-NCC. PS1=pseudo-first-order kinetic model; PS2=pseudo-second-order kinetic model. (Adsorbent dose 0.800 g/L; pH 5.2)

Figure 8a-c. Langmuir and Freundlich isotherm modeling: a) Cd^{2+}, b) Ni^{2+} and c) PO_4^{3-} adsorption onto CHABENT-MFC (Adsorbent dose 0.800 g/L; pH 5.2, time 12 h).

Figure 9. The removal efficiency after regeneration metals with 0.10 M HNO_3 and PO_4^{3-} with 0.10 M NaOH. (Adsorbent dose 0.800 g/L; pH 5.2)

Table 1. Kinetic parameters of Cd^{2+}, Ni^{2+} and PO_4^{-3} adsorption onto CHA-BENT-NCC.

	q_e	Pseudo-first-order			Pseudo-second-order		
Type of contamintns	(mmol/g)	q_t (mmol/g)	k_1 (1/min)	R^2	q_t (mmol/g)	k_2 (g/mg* min)	R^2
Cd^{2+}	1.265	0.956	2.651	0.466	1.282	7.878	0.656
Ni^{2+}	1.241	1.264	1.583	0.695	1.286	1.585	0.852
PO_4^{-3}	0.817	0.956	0.148	0.864	1.016	0.264	0.865

Table 2. Langmuir and Freundlich parameters for Cd^{2+}, Ni^{2+} and PO_4^{-3} adsorption by CHA-BENT-NCC.

Langmuir					***Freundlich***		
Adsorbate	$q_{m,exp}$ **(mmol/g)**	q_m**(mmol/g)**	K_L	R^2	n_F	K	R^2
Ni^{2+}	22.96	29.15	2.13	0.90	2.04	20.07	1.00
Cd^{2+}	9.71	10.34	64.15	0.96	2.17	28.38	0.97
PO_4^{3-}	3.96	4.90	0.71	0.77	1.60	1.92	0.90

Table 3. Comparison of the maximum metal and phosphate adsorption capacities for some cellulose based materials.

Sorption material	Adsorbate	Capacity (mmol/g)	Ref.
TEMPO—oxidatadet	Ni^{2+}	0.15	
CNF	Cd^{2+}	0,09	[16]
Cellulose-ZnO_2	Ni^{2+}	4.95	
	Cd^{2+}	0.57	[20]
	Fe^{3+}	0.89	
	Zr^{4+}	0.70	
	Cu^{2+}	0.58	
	Cd^{2+}	0.57	
	Cr^{3+}	0.45	
	Zn^{2+}	0.41	
	Co^{2+}	0.36	
Carboxymethyl	Cu^{2+}	6.49	
cellulose	Ni^{2+}	4.06	[17]
	Pb^{2+}	5.15	
	PO_4^{3-}	0.23	
Cellulose/Metal			[13]
Hybrid Macrogels			

Reduced iron oxide impregnated wood	PO_4^{3-}	1.38	[47]
Magnesium silicate-hydrothermal carbon composite	Cd^{2+}	3.74	[18]
Chitin-Cellulose beds	Pb^{2+}	0.33	
	Cd^{2+}	0.32	[14]
	Cu^{2+}	0.30	
Composites synthesized from cellulose and crown ether	Ni^{2+}	3.20	
	Cd^{25}	1.76	[7]
Acrylamide grafted cellulose	Cd^{2+}	3.12	[8]
Oxolane-2,5-dione functionalized NC	Pb^{2+}	0.59	[15]
	Cd^{2+}	1.21	
CHA-BENT-NCC	Ni^{2+}	29.46	(This work)
	Cd^{2+}	10.34	
	PO_4^{3-}	4.90	

Table 4. Thermodynamic parameters of Cd^{2+}, Ni^{2+} and PO_4^{3-}.

	T(K)	ΔH(kJ/mol)	ΔS (J/mol K)	ΔG (kJ/mol)	R^2	Adsorption efficiency (%)
	290			-14.90		99.3
Cd^2	296	0.08	0.05	-15.15	0.994	99.5
	308			-21.10		99.5
	290			-10.60		98.2
Ni^{2+}	296	0.13	0.40	-12.00	0.989	99.0
	308			-17.25		99.8
	290			-3.29		72.0
PO_4^{3-}	296	16.64	53.33	-4.44	0.998	80.0
	308			-6.64		89.8

Table 5. Composition of mining wastewater from a copper mine before and after treatment using CHA-BENT-NCC adsorbent.

Studied metal ions	Before treatment (mmol/g)	After treatment (mmol/g)
Cu^{2+}	1.72	0.01
Ni^{2+}	0.03	0.00
Zn^{2+}	90.77	0.30
Fe^{3+}	60.87	0.22

Highlights:

- Ecofriendly composite material for water treatment
- Rapid and efficiency adsorption material
- Possible to remove cationic and anionic ions by same material and simultaneously
- Simple synthesis route

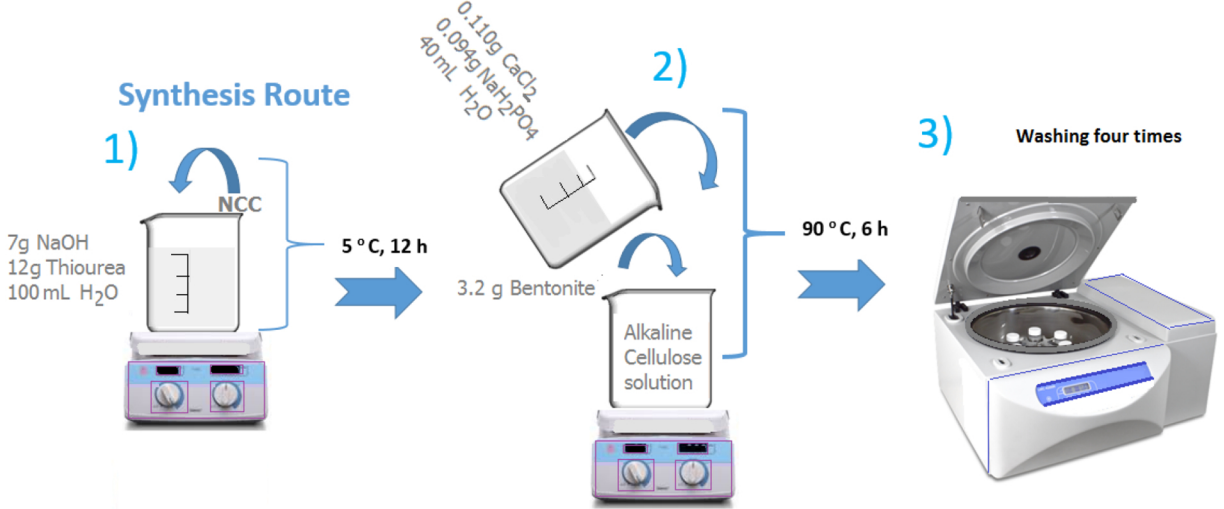
Synthesis Route
1)
NCC
7g NaOH
12g Thiourea
100 mL H_2O
5 °C, 12 h
0.110g $CaCl_2$
0.094g NaH_2PO_4
40 mL H_2O
2)
3.2 g Bentonite
Alkaline
Cellulose
solution
90 °C, 6 h
3)
Washing four times

Figure 1

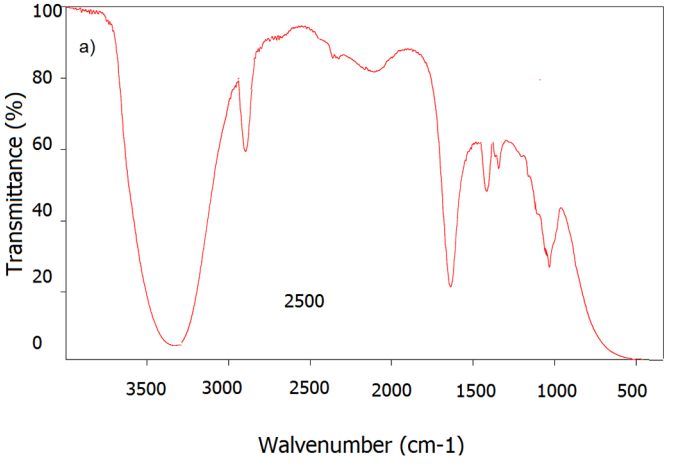

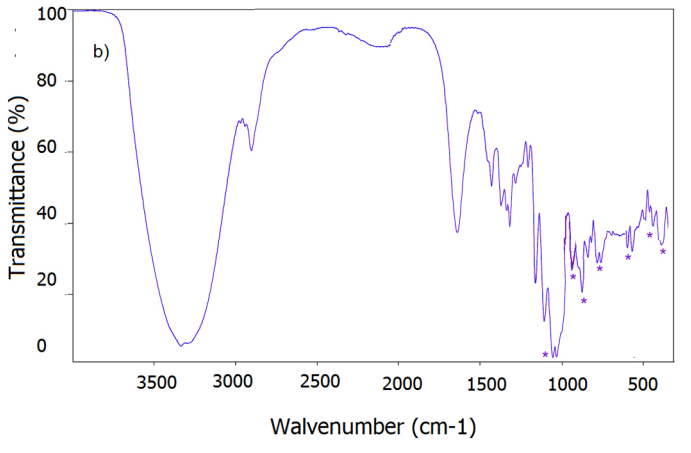

Walvelenght (cm^{-1})	Process
3300	O-H stretching
2900	C-H stretching in cellulose
1640	The bending mode of H-OH in water
1435	C-H and O-C-H in-plane bending vibration
1360	C-H deformation
1060	C-O-C pyranose ring skeletal vibration
960-1025 *	The stretching vibrations of PO_4^{3-}
890 *	C-O-C, C-C-O and C-C-H deformation modes and stretching vibrations
690-790 *	Si-O stretching and vibration
600-620 *	Al-O and Si-O out of plane vibration
550 *	Al-O-Si deformation
490 *	Si-O-Fe deformation
470 *	Mg-O deformation

Figure 2

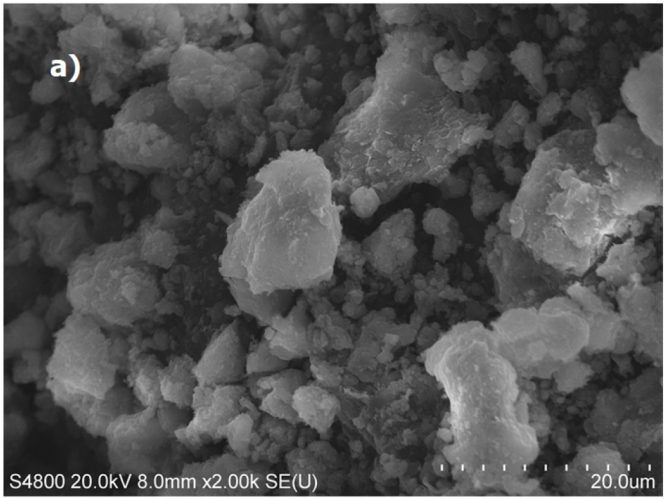

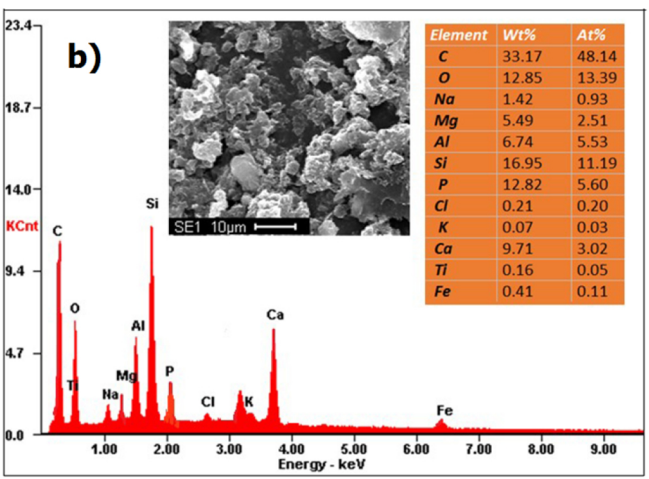

Element	Wt%	At%
C	33.17	48.14
O	12.85	13.39
Na	1.42	0.93
Mg	5.49	2.51
Al	6.74	5.53
Si	16.95	11.19
P	12.82	5.60
Cl	0.21	0.20
K	0.07	0.03
Ca	9.71	3.02
Ti	0.16	0.05
Fe	0.41	0.11

Figure 3

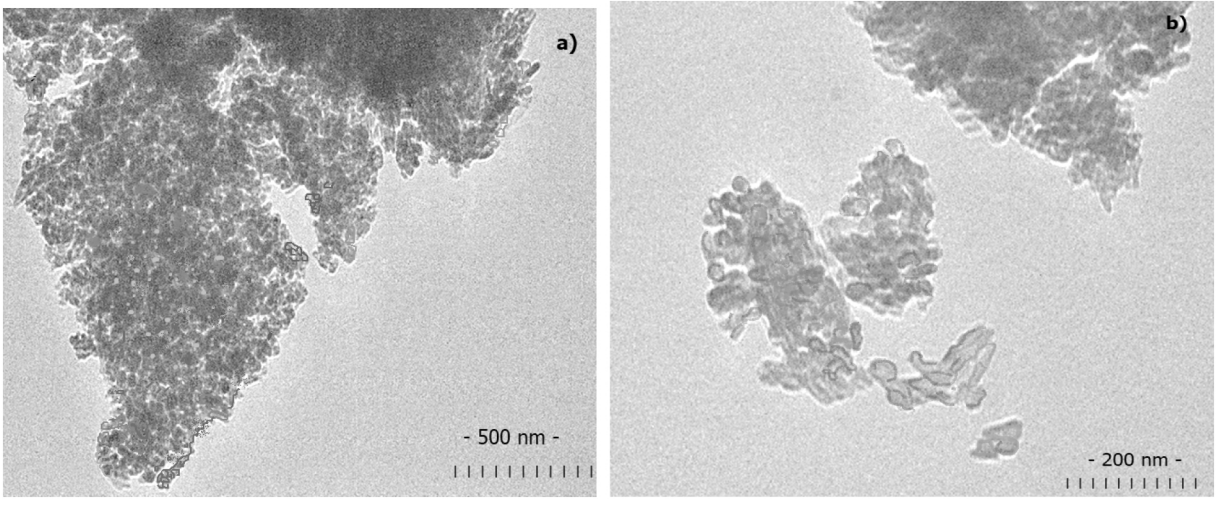

Figure 4

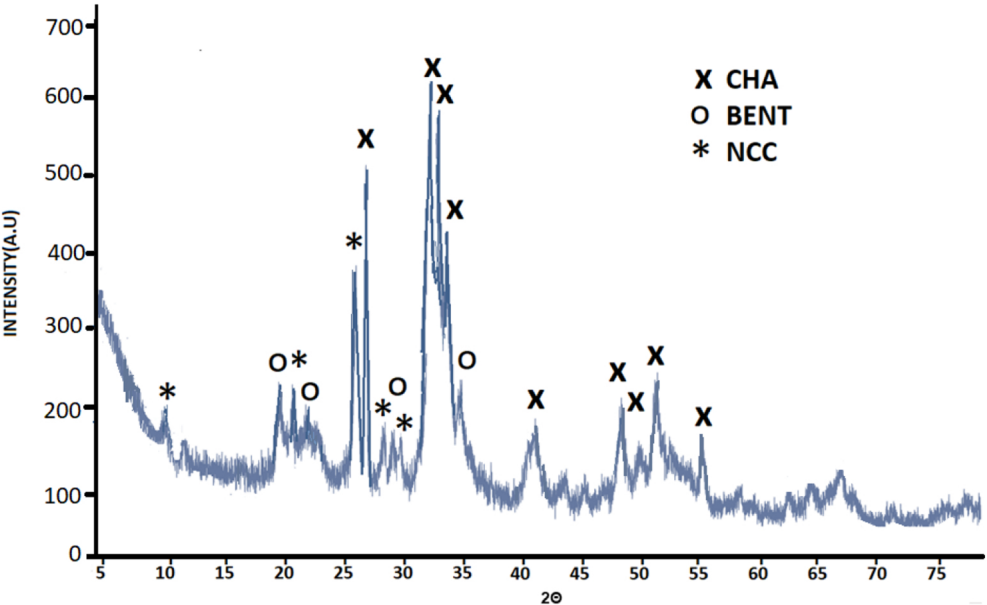
X CHA
O BENT
* NCC
INTENSITY(A.U)
2Θ
0
100
200
300
400
500
600
700
5
10
15
20
25
30
35
40
45
50
55
60
65
70
75

Figure 5

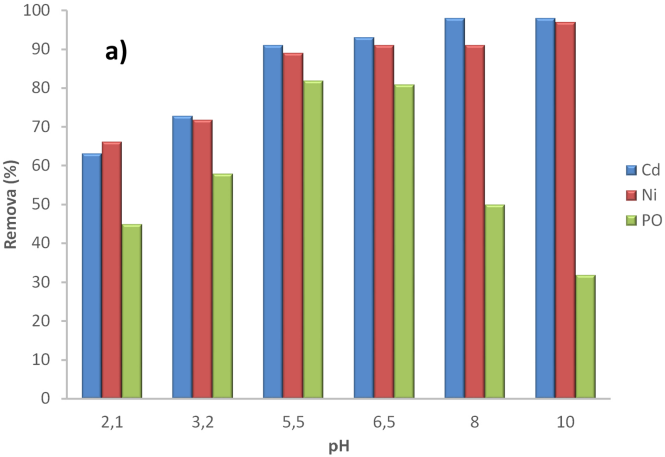
a)
Remova (%)
100
90
80
70
60
50
40
30
20
10
0
2,1
3,2
5,5
6,5
8
10
pH
Cd
Ni
PO

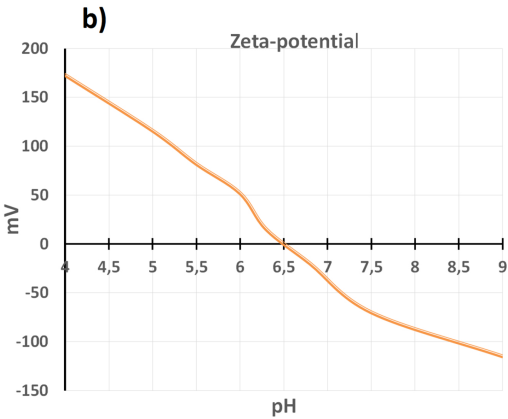
b)
Zeta-potential
mV
200
150
100
50
0
-50
-100
-150
4
4,5
5
5,5
6
6,5
7
7,5
8
8,5
9
pH

Figure 6

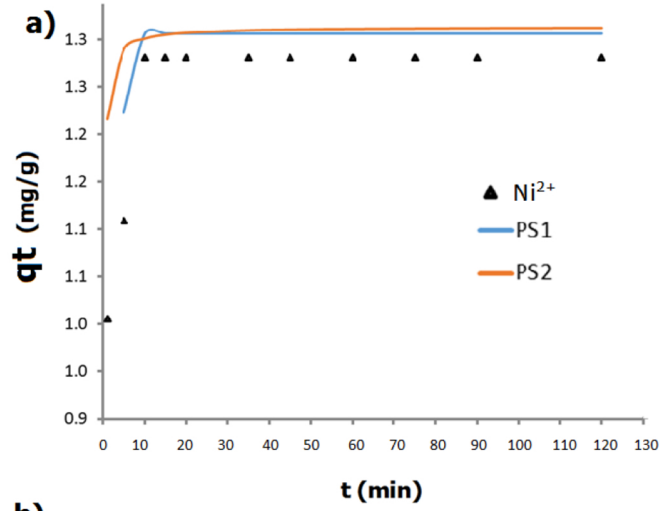
a)
qt (mg/g)
t (min)
Ni2+
PS1
PS2

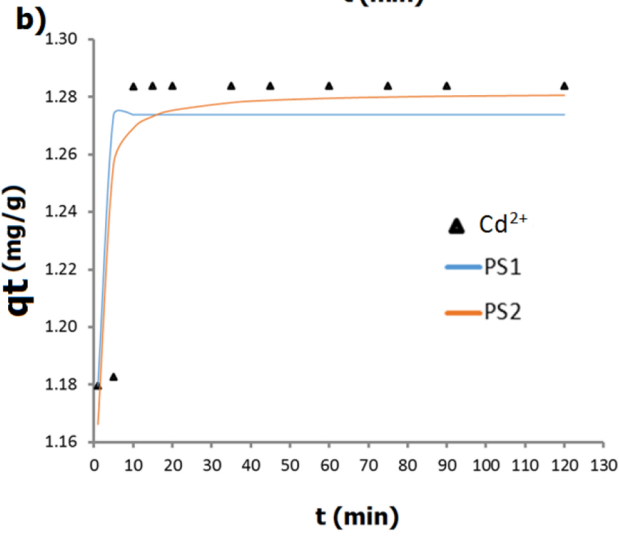
b)
qt (mg/g)
t (min)
Cd2+
PS1
PS2

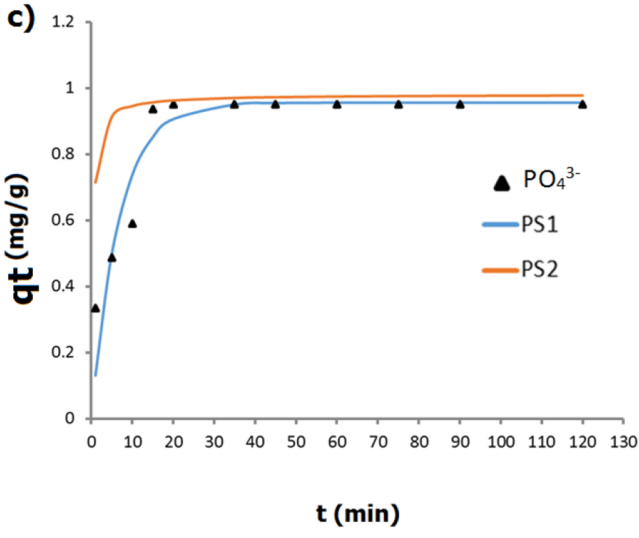
c)
qt (mg/g)
t (min)
PO43-
PS1
PS2

Figure 7

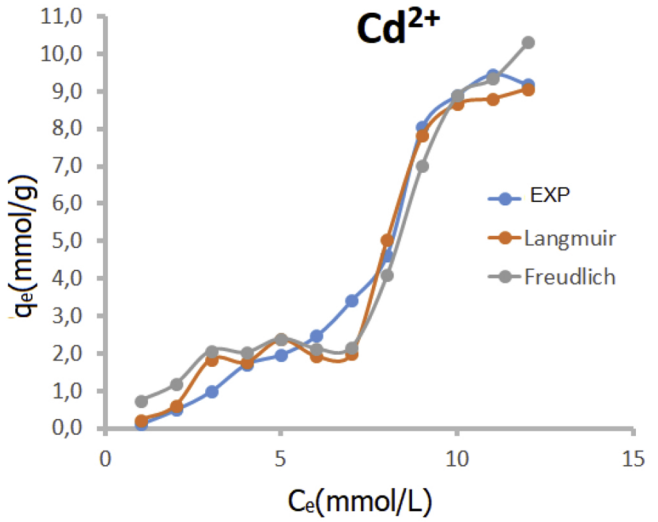
Cd2+
qe(mmol/g)
Ce(mmol/L)
EXP
Langmuir
Freudlich

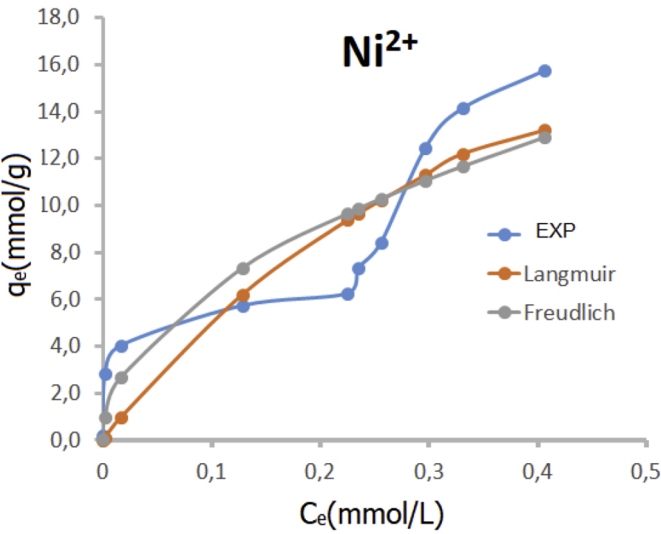
Ni2+
qe(mmol/g)
Ce(mmol/L)
EXP
Langmuir
Freudlich

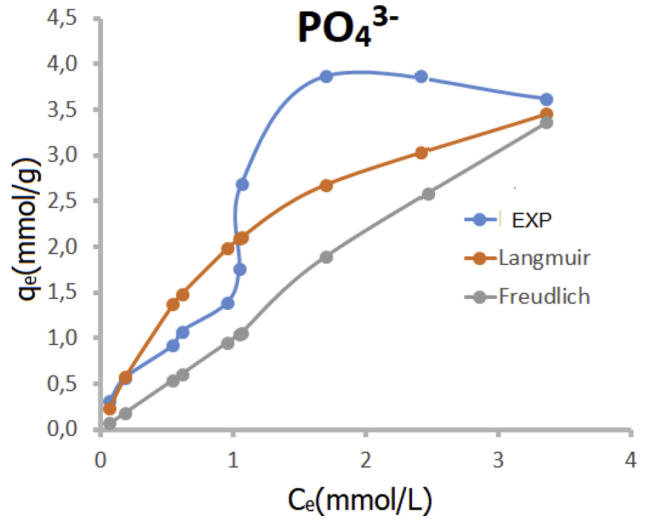
PO43-
qe(mmol/g)
Ce(mmol/L)
EXP
Langmuir
Freudlich

Figure 8

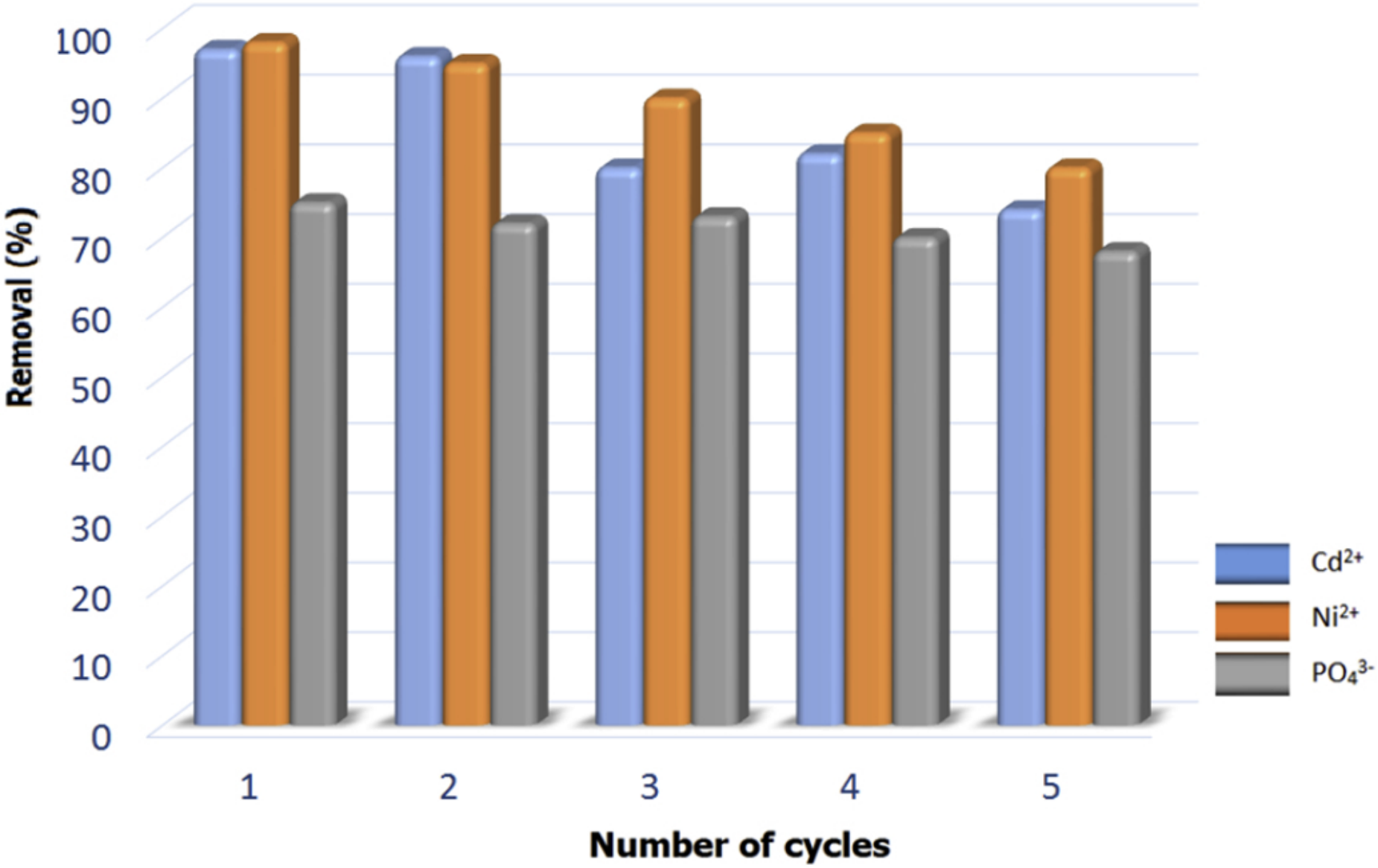
Removal (%)
100
90
80
70
60
50
40
30
20
10
0
1
2
3
4
5
Number of cycles
Cd2+
Ni2+
PO43-

Figure 9